Role of NO delta+ Intermediates in NO Reduction with Propene over NiZSM-5 Zeolite Revealed by EPR and IR Spectroscopic Investigations and DFT Modeling

ARTICLE *in* THE JOURNAL OF PHYSICAL CHEMISTRY C · JULY 2011

Impact Factor: 4.77 · DOI: 10.1021/jp203188k

3 AUTHORS:

Piotr Pietrzyk
Jagiellonian University
45 PUBLICATIONS **509** CITATIONS
SEE PROFILE

Katarzyna Podolska-Serafin
Jagiellonian University
8 PUBLICATIONS **46** CITATIONS
SEE PROFILE

Zbigniew Sojka
Jagiellonian University
206 PUBLICATIONS **2,090** CITATIONS
SEE PROFILE

THE JOURNAL OF PHYSICAL CHEMISTRY C

ARTICLE

pubs.acs.org/JPCC

Role of $NO^{\delta+}$ Intermediates in NO Reduction with Propene over NiZSM-5 Zeolite Revealed by EPR and IR Spectroscopic Investigations and DFT Modeling

Piotr Pietrzyk,* Katarzyna Podolska, and Zbigniew Sojka

Faculty of Chemistry, Jagiellonian University, ul. Ingardena 3, 30-060 Krakow, Poland

ABSTRACT: Adsorption at variable temperatures of individual components (NO, NO_2, CO, O_2, C_3H_6) and their mixtures simulating the feed of the selective catalytic reduction (SCR) of NO_x with propene over NiZSM-5 catalysts was investigated by electron paramagnetic resonance, infrared, and mass spectroscopies to provide direct insights into the nature of the primary reaction intermediates and alternation of the valence state of the nickel centers. The key intermediates ($\{Ni-NO\}^{2+}$, $\{Ni^{+}-C_3H_6\}$, $\{Ni^{+}-(CO)_n\}$, and $\{Ni^{2+}-O_2^{-}\}$) relevant to the SCR process were isolated and identified, and their structure together with spectroscopic signatures were ascertained by parallel density functional theory molecular modeling. Alternation of the nickel valence state during the SCR reaction, leading to formation of a Ni^{2+}/Ni^{+} redox couple, was triggered by the reductive adsorption of NO and oxidative adsorption of O_2. The sequence at which the reactant molecules were reactively coordinated was dictated by the oxidation state of the nickel centers. It was shown that the SCR process is initiated by chemoselective capture of NO from the reaction mixture by oxidized nickel sites. Concerted spin-pairing and ligand-to-metal charge-transfer events involved in this process lead cooperatively to the formation of nickel-bound nitrosonium ($NO^{\delta+}$) species as the prime intermediate. At SCR temperatures (above 673 K), $NO^{\delta+}$ in the presence of propene and dioxygen is readily converted into N_2, CO_x, and H_2O, the final products of the SCR reaction.

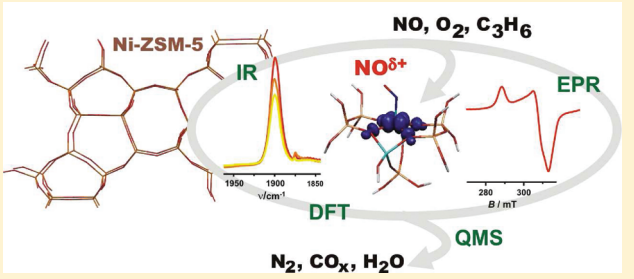

1. INTRODUCTION

Mitigation of anthropogenic nitric oxides is usually achieved by direct decomposition ($deNO_x$)[1−3] or by selective catalytic reduction with ammonia (NH_3-SCR) or hydrocarbons (HC-SCR).[4−7] In direct decomposition of NO_x, the presence of oxygen retards appreciably the reaction progress. On the contrary, when hydrocarbons are applied as reducing agents, oxygen can enhance advancement of the SCR process in a remarkable way when an appropriate catalyst is used. For a given catalyst, the temperature of the highest NO conversion depends on the type of the hydrocarbon reductor, the zeolite morphology, and its Brönsted acidity.[8−10] Yet, a possible synergistic effect of the metallic and protonic sites, postulated by some authors,[10] has not been clarified definitely. The prime role of the catalyst is to ensure preferential oxidation of the hydrocarbons by the nitric oxide related surface (NO_2^{-}, NO_3^{-}, NO^{+}) and gas-phase (NO_2) intermediates suppressing at the same time a competitive pathway where hydrocarbons react incipiently with the surplus oxygen.

The surface NO_2^{-} and NO_3^{-} species produced upon the interaction of NO with O_2 exhibit intense, broad IR absorption bands in the region of 1470−1200 cm^{-1} and 1650−1500 cm^{-1}, respectively.[11] Their detailed assignment to the well-defined molecular structures is still not explicit because of the profuse speciation into various bridging, bidentate, or monodentate surface nitrates and nitrites. There are only a few attempts to address this issue by density functional theory (DFT) modeling[12−14] in comparison to more abundant literature on the quantum chemical calculations of intrazeolitic mono- and dinitrosyl structures.[15−17]

The surface nitrosonium (NO^{+}) species have been revealed by in-situ Fourier transform infrared (FTIR) spectroscopy (ν = 2133 cm^{-1}) on HZSM-5 and partially exchanged MHZSM-5 zeolites (M = Cu, Co, Fe) under the flow of NO and O_2 mixture. Their appearance is usually accounted for by the reaction involving Brönsted acid sites: $2NO + 1/2O_2 + 2H_{zeol}^{+} \rightarrow 2NO_{zeol}^{+} + H_2O$.[2,4,9] Nevertheless, the NO^{+} species can also be formed upon reductive adsorption of nitric oxide on transition-metal ions ($NO + Me_{zeol}^{n+} \rightarrow NO_{zeol}^{+} + Me_{zeol}^{(n-1)+}$) heterogenized in zeolites,[18−20] but mechanistic relevance of such a process has not yet been discussed.

There is some consensus about the gross mechanistic steps of the SCR reaction entailing oxidation of NO to surface nitrates, nitrites, and nitrosonium species, which in the presence of hydrocarbons produce various organic nitro-, nitrile-, and cyanide or isocyanate compounds.[2,4,9,21] Upon interaction with NO_x and O_2, they are converted into N_2, CO_2, and H_2O with one N-atom coming from the nitrogenated organic intermediate and the other from NO_x as revealed by previous studies using ^{15}N-enriched reactants.[2] In the presence of water, the isocyanates

Received: April 6, 2011
Revised: June 1, 2011
Published: June 02, 2011

can also be hydrolyzed into ammonia, and the latter species has been claimed sometimes to actually reduce NO_x to N_2.[22] Nonetheless, despite extensive investigations, the mechanism of HC-SCR reaction is still a matter of vivid discussions, and several important surface events and their molecular aspects need to be further clarified. In particular, the questions of which oxidant, NO^+, NO_2^-/NO_3^-, or NO_2, plays a prime role in the hydrocarbon activation and of how the valence state of the metal active sites may influence the sequence of the reaction elementary steps are apparently of the utmost mechanistic importance.

Various metallo-zeolites containing exchanged transition-metal ions such as Cu,[16,23,24] Fe,[25] Co,[4,19,26] or Ni[10,18,27] exhibit remarkable activity in the SCR process. In this context, the Ni-containing zeolites have attracted considerable attention because of their ability to promote the reaction with both the unsaturated and saturated hydrocarbons including methane.[10,28−30] It is tacitly accepted that those cations change their oxidation states during the reaction progress.[19,23,31] Another peculiarity of the SCR reaction is a dramatic redistribution of the spin density when passing from the reactants to the products (both NO ($^2\Pi_{1/2}$) and NO_2 ($^2A_1$) molecules are spin doublets, whereas N_2 ($^1\Sigma_g^+$) is diamagnetic and O_2 ($^3\Sigma_g^-$) is a spin triplet species) leading to the appearance of paramagnetic intermediates.[32] Lately, we have pointed out the importance of the oxidation and the spin state of cobalt centers dispersed in MFI and BEA zeolites for reactions with nitrogen oxides.[19] It has been shown that the NO molecule exhibits high ligation affinity to the oxidized cobalt sites, while the olefin or CO ligands exhibit it to reduced ones. It is, therefore, of great mechanistic importance to elucidate the actual valence and spin states of the metal active sites and the reacting species and their alternation in the course of the HC-SCR reaction. In the vast majority of cases, surface intermediates of the SCR reaction have been examined by IR spectroscopy.[9−11,21,30,33] For that reason, because of the inherent limitations of this technique, any direct insight into the redox processes induced by electron transfer between the active site and the gaseous reactants, resulting in the formation of various radical intermediates, is obviously restricted. On the contrary, this aspect of SCR activity can be probed quite effectively with electron paramagnetic resonance (EPR) techniques.[18−20,34−36]

The aim of this work was to study by means of EPR in conjunction with IR and DFT calculations the interaction of nickel-exchanged ZSM-5 zeolites with the principal reactants of the SCR process (NO_x, CO, O_2, and C_3H_6) adsorbed separately or together. Particular attention was focused on the less investigated influence of the metal valence state on the ligation affinity toward the oxidant (NO_x, O_2) and the reductant (C_3H_6, CO) molecules and elucidation of the mechanistic role of the $NO^{\delta+}$ intermediate.

2. MATERIALS AND METHODS

2.1. Materials. Ni-exchanged zeolite catalysts were obtained by standard ion exchange procedure from parent ammonium forms of ZSM-5 (Zeolyst, Inc.) samples with the Si/Al ratio equal to 15 and 40 and 0.1 M $Ni(NO_3)_2$ aqueous solution. The final pH of the solution varied from 2 to 5. Chemical analysis by means of atomic absorption spectroscopy with inductively coupled plasma (AAS-ICP) method revealed the Ni/Al exchange degrees of 54 and 40%, respectively. After drying, prior to the measurements and adsorption of gas reactants (NO, NO_2, CO, O_2, and C_3H_6), the samples were activated in a vacuum of 10^{-5} mbar at 773 K for 2 h (heating rate of 6 K/min). Before adsorption, NO (Aldrich) was purified by the freeze−pump−thaw technique, whereas CO, O_2, and propene (Aldrich) were used without prior purification.

2.2. Characterization. CW-EPR spectra were recorded with a Bruker ELEXSYS-500 X-band spectrometer with the 100 kHz field modulation equipped with a nitrogen variable temperature unit. The microwave power of 1−100 mW and the modulation amplitude of 0.2−0.5 mT were applied. The spectra processing was performed with the software provided by Bruker, while for computer simulation of the powder spectra the EPRsim32[37] program was used. In-situ variable temperature measurements with quadrupole mass spectrometry (QMS) analysis of the products were carried out directly in the EPR quartz tubes using a RGA200 quadruple mass spectrometer (Stanford Research System). IR studies of NO and CO adsorption on the Ni-zeolites were recorded with a Tensor 27 spectrometer (Bruker) equipped with the mercury cadmium telluride (MCT) detector using a homemade quartz cell connected to vacuum line (with the background pressure of 10^{-5} mbar).

2.3. DFT Modeling. Interaction of nickel cations with the zeolite framework and formation of the adsorption complexes was studied by means of DFT methods implemented in the ADF package.[38] Cluster calculations were carried out for both parent Ni^{2+}ZSM-5 and Ni^+ZSM-5 nickel centers followed by modeling of the nitrosyl $\{NiNO\}^{2+}$ZSM-5, carbonyl $\{Ni(CO)_n\}^+$ZSM-5 ($n = 0 \div 4$), and dioxygen $\{NiO_2\}^+$ZSM-5 adducts. The ZSM-5 hosting sites were modeled with a cluster of the $Si_6AlO_8(OH)_{12}^-$ stoichiometry referred to as M7.[16] Geometry optimization was performed within the Kohn−Sham formalism using a gradient-corrected BP86 functional and a TZV basis set.[39] The structure of the cluster models were optimized with analytic gradients and BFGS method within the SCF electron density convergence criterion of 10^{-6} au, a gradient criterion of 10^{-3} au/Å, and a maximum displacement criterion of 10^{-3} Å. For the experimental cage complexes of nickel for which spectroscopic parameters were determined, vibrational analysis and calculation of EPR signatures were carried out. The frequency calculations were based on the harmonic approximation, whereas the magnetic parameters ($\boldsymbol{g}$ and hyperfine $\boldsymbol{A}$ tensors) were calculated with ORCA software[40] employing relativistic spin−orbit mean field (SOMF)[41] approximation of the spin−orbit effects and the hybrid B3LYP functional.[42]

3. RESULTS AND DISCUSSION

3.1. Interaction of Ni^{2+}ZSM-5 with Single SCR Reactants. To register all accessible nickel centers and to reveal possible adsorption modes of the SCR reactants, initial spectroscopic experiments were performed at low temperatures. The EPR spectrum of the oxidized NiZSM-5 sample, recorded at 77 K (Figure 1a), exhibits only a weak narrow line (g_{iso} = 2.003) usually assigned to the residual carbon radicals or defect centers in the zeolite framework. The absence of any signal attributable to the intrazeolitic nickel ions is in accordance with their divalent (Ni^{2+}) high spin state ($3d^8$, S = 1), which is undetectable at conventional X-band CW-EPR because of the large zero-field splitting. This is consistent with DFT modeling, which showed that Ni^{2+} ions accommodated in the M7 sites, indeed, exhibiting a triplet spin ground state. The calculated zero-field splitting parameters (BP-SOMF-QRO)[43] are equal to D = 14.2 cm^{-1} and E = 0.9 cm^{-1}, which are in line with the values observed for the 4-fold molecular nickel(II) complexes.[44] Adsorption of C_3H_6 at temperatures below 400 K did not lead to formation of any new EPR signal indicating a quite low affinity of the oxidized Ni^{2+}

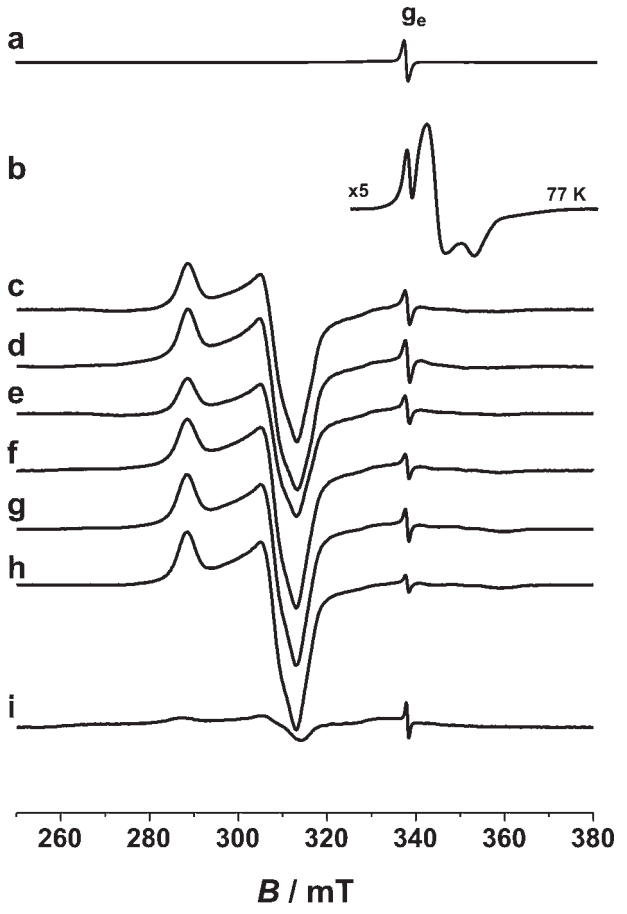

Figure 1. X-band EPR spectra recorded at 77 K of the activated NiZSM-5 sample (a) and after adsorption of 10 Torr of NO (b−i). (b) Enlarged part of the EPR spectrum after NO adsorption at 77 K, (c−h) evolution of the EPR signal upon heating from 273 to 773 K, and (i) signal after evacuation of the sample at 773 K.

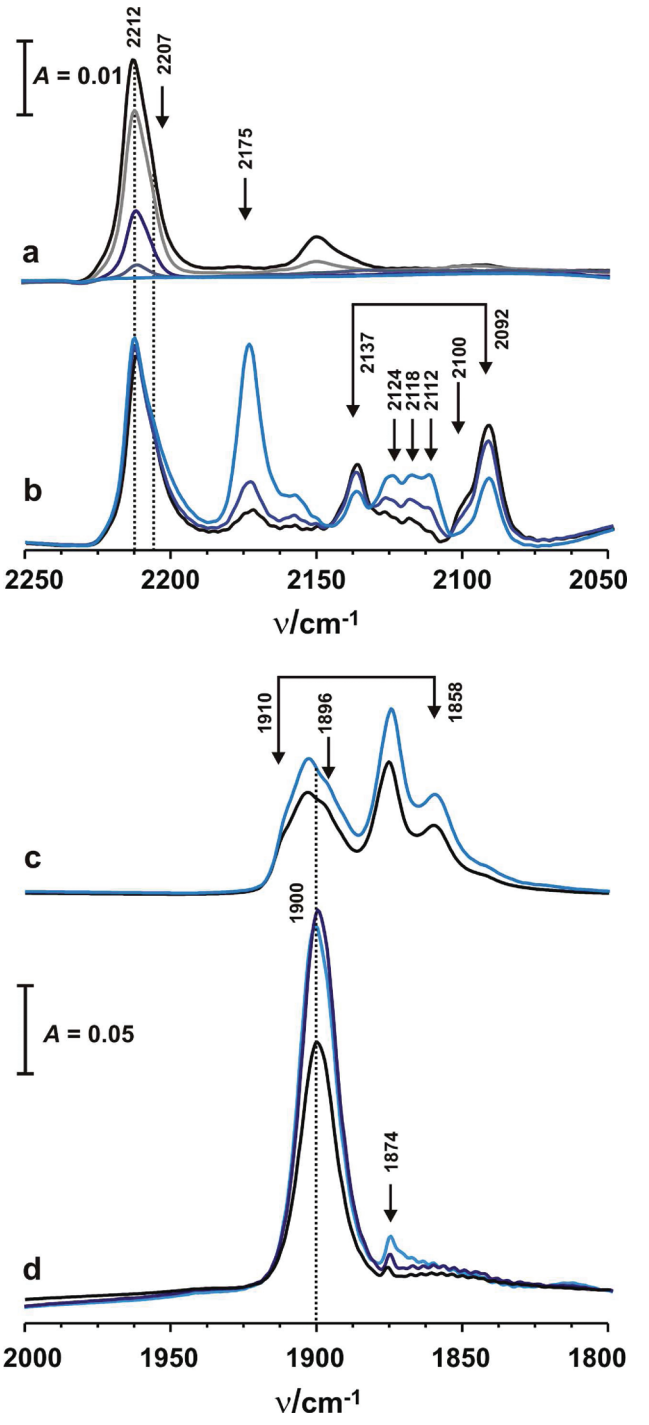

Figure 2. FTIR spectra of (a) CO desorption at 373 K from activated NiZSM-5 followed by (b) CO adsorption on reduced NiZSM-5 (a prior reduction at 773 K for 15 min in CO). FTIR spectra of (c) NO adsorbed on thermally activated NiZSM-5 obtained after sequential NO adsorption at 153 K followed by (d) subsequent evolution of the signal under dynamic vacuum from 383 to 773 K.

sites to reductive adsorption of propene in this temperature window reported previously for an analogous CoZSM-5 catalyst.[19] Above this temperature, an appreciable reduction of Ni^{2+} to Ni^{+} was observed with the maximum EPR intensity at 580 K. A similar result (lack of any new EPR signal) was obtained in the case of CO adsorption below 450 K. Indeed, parallel IR spectra (Figure 2a) revealed a simple ligation of carbon monoxide to divalent nickel upon adsorption at room temperature without any alternation of the metal valence state. The bands at ν = 2212 and 2207 cm^{-1} (the latter is better seen in Figure 2b) were clearly associated with two kinds of $\{Ni^{2+}-CO\}$ species consistent with two topological types of the parent nickel ions, whereas dicarbonyl adducts of nickel(II), characterized by very low stability, were formed exclusively at cryogenic temperatures (around 100 K) in excess of CO in accordance with previous literature.[45] In general, these complexes were labile as the most stable monocarbonyls of nickel(II) were easily destroyed already at 373 K (Figure 2a), that is, well below the onset of the SCR reaction. The bands at 2175 and 2148 cm^{-1} are due to CO interacting with OH groups and CO occluded within the zeolite pores, respectively.[45]

In contrast to propene and carbon monoxide, adsorption of nitric oxide on the Ni^{2+}ZSM-5 samples led to an immediate appearance of two types of orthorhombic EPR signals (Figure 1b, c) of which the intensity depended on the NO pressure and the adsorption temperature. The weaker signal at the high field part of the spectrum (Figure 1b) with g_{xx} = 1.993, g_{yy} = 1.975, and g_{zz} = 1.922 and with unresolved hyperfine structure due to $^{14}N(I = 1, 99.63\%)$ is typical of surface-trapped NO radicals. A noteworthy feature of this signal is a distinct hipsomagnetic shift of the g_{zz} component with respect to

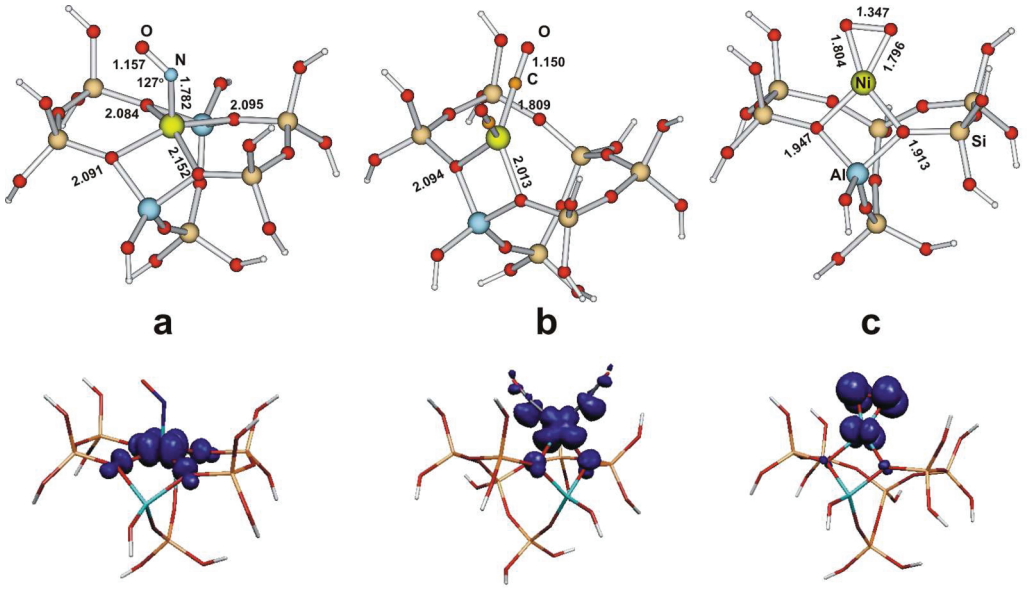

Figure 3. DFT optimized molecular models and the corresponding spin density contours of the representative intrazeolitic complexes involved in SCR process over NiZSM-5 catalyst: (a) $\{Ni{-}NO\}^{2+}$M7, (b) $\{Ni^{+}{-}(CO)_2\}$M7, and (c) $\{Ni^{2+}{-}O_2^{-}\}$M7. Bond lengths are given in angstroms.

$g_e = 2.0023$ value indicating that the unpaired electron is retained on the NO moiety upon adsorption. Such $\boldsymbol{g}$ tensor can be accounted for by a perturbed $^2\Pi_{1/2}$ radical with SOMO defined by the $2\pi^*_g$ orbital stabilized by the interaction with surface Lewis sites, L_{Al}, constituted by the Al ions.[46] The local symmetry of the NO admolecule must be rhombic (or lower) since an axial crystal field cannot lift the degeneracy of the $2\pi_g^*$ levels. This is consistent with a bent geometry ($L_{Al}{-}N{-}O$ angle smaller than 180°) of the adsorbed NO molecule allowing for effective quenching of the orbital magnetic moment, which is a necessary condition for straightforward EPR detection of such adsorption mode.[18] The $\{NO{-}L_{Al}\}$ species are unstable under the temperature and evacuation (vide infra) and are, therefore, irrelevant for the SCR process.

The much more intense EPR signal at the low part of the magnetic field (Figure 1c) exhibits completely different parameters with pronounced batomagnetic shift of all g_{ii} components with respect to the g_e value. Computer simulation revealed the presence of at least two constituent signals with the following spin-Hamiltonian parameters: $g_{xx}^1 = 2.157$, $g_{yy}^1 = 2.200$, $g_{zz}^1 = 2.355$, $g_{xx}^2 = 2.145$, $g_{yy}^2 = 2.233$, $g_{zz}^2 = 2.370$. Such a $\boldsymbol{g}$ tensor is characteristic of a metal-centered paramagnet with the $3d^9$ electron configuration, such as that of Cu^{2+}ZSM-5.[23] Thus, the observed $\boldsymbol{g}$ tensor components indicate severe modification of the electronic structure of the NO molecule upon adsorption on the nickel sites. Following our previous studies, we assign this signal to the adducts of the type $\{Ni{-}NO\}^{2+}$ZSM-5 ($S = {}^1/_2$, $3d^9$).[18] However, the $\{Ni{-}NO\}^{2+}$ notation indicates merely the formal total oxidation state of the metal Ni^+ (d^9) and ligand NO^+ (π^{*0}_{2p}) moieties upon NO adsorption on Ni^{2+} sites, which obviously is not tantamount with the actual partial charge redistribution. The latter is closer to $\{Ni^{(2-\delta)+}{-}NO^{\delta+}\}$ formulation, and the degree of the charge transfer is dictated by the relative position of the NO π^{*1}_{2p} donor level with respect to the semioccupied Ni $3d_z^2$ acceptor one (σ donation channel) and the position of the occupied $3d_{xz}$ orbital in comparison to the empty level π^{*0}_{2p} (π back-donation channel). As the bare nickel(II) centers exhibit triplet spin state (vide supra), the nitrosyl adducts with spin doublet state are apparently formed via spin-pairing mechanism accompanied by partial ligand-to-metal electron-transfer (LMET) process (indicated by the blue shift of the nitrosyl IR band). Both mechanisms lead jointly to formal reduction of the nickel(II) sites to nickel(I) with concomitant oxidation of the coordinated NO molecule to NO^+ (actually $NO^{\delta+}$). The nitric oxide ligand is thereby transformed into the electrophilic nitrosonium $NO^{\delta+}$ species of high oxidation properties following the reaction

$$^2NO + {}^3Ni^{2+}ZSM\text{-}5 \rightarrow {}^2\{Ni{-}NO\}^{2+}\ ZSM\text{-}5 \qquad (1)$$

Similar behavior was observed for dinitrosyl species of cobalt(II) ($S = 3/2$, $3d^7$), where spin-transfer process led to a formal Co^0 ($3d^9$) state of cobalt sites manifested by the characteristic EPR $\boldsymbol{g}$ tensor.[19]

Parallel DFT calculations revealed that binding of the NO molecule takes place via expansion of the coordination sphere giving rise to a bend adduct with the Ni−N−O angle of 127° and the Ni−NO bond length of $d_{Ni-NO} = 1.782$ Å. The optimized geometry of the $\{Ni{-}NO\}^{2+}$M7 model is shown in Figure 3a. The metal−ligand interaction is rather strong with the calculated adsorption energy of $\Delta E_{ads} = -26$ kcal/mol. Despite the significant activation, the N−O distance ($d_{NiN-O} = 1.157$ Å) was shortened only slightly with respect to the gas-phase value ($d_{N-O} = 1.166$ Å). The calculated $\boldsymbol{g}$ tensor ($g_{xx} = 2.187$, $g_{yy} = 2.227$, $g_{zz} = 2.284$) remains in a reasonable agreement with the experiment. Repartition of the spin density within the $\{Ni{-}NO\}^{2+}$ unit revealed by means of the restricted-open-shell DFT calculations indicates that the unpaired electron is confined to the metal core ($\rho(d_{xy}) = 0.72$, $\rho(d_{yz}) = 0.11$) in accordance with the spin-pairing pathway of the NO adsorption $\{\uparrow Ni\uparrow{-}\downarrow NO\}$. A similar picture of the NO binding to surface Ni^{2+} sites was earlier proposed for the NiO/MgO system.[47] In addition, the positions of the mononitrosyl bands in the IR spectra at $\nu = 1902$ and 1896 cm^{-1} (Figure 2c), which are blue-shifted with respect to the gas-phase value (1874 cm^{-1}), indicate depopulation of the $2\pi^*_g$ state and formulation of the bound $NO^{\delta+}$ nitric oxide moiety in conformity with the EPR results.

dx.doi.org/10.1021/jp203188k |J. Phys. Chem. C 2011, 115, 13008–13015

The presence of a doublet band located at 1910 and 1858 cm^{-1} is characteristic of the diamagnetic nickel dinitrosyls $\{Ni^{2+}-(NO)_2\}$ZSM-5.[30,33] Evacuation of the sample up to 773 K resulted in disappearance of the dinitrosyl bands and a consequent increase of the 1900 cm^{-1} band because of the mononitrosyl species (Figure 2d). A small shift of 2 cm^{-1} with respect to the spectrum recorded at room temperature (1902 cm^{-1}) is due to thermal dynamic effects. Interestingly, adsorption of NO_2 led to a virtually identical EPR signal (spectra not shown) as that observed after NO adsorption (Figure 1c). Thus, interaction with NO_2 presumably leads to the formation of a η^1-N adduct and the transfer/spin pairing of the electron from the half-occupied sp^2 hybrid pointing toward nickel center, which apparently is accompanied by dissociation of one of the N−O bonds. Such dissociative adsorption of NO_2 on ionic oxides and zeolites exchanged with transition-metal ions has been observed previously.[48]

Upon stepwise increase of the temperature above 290 K, the EPR signal due to NO adsorbed on the Lewis acid sites immediately vanished, whereas that assigned to the mononitrosyl $\{Ni-NO\}^{2+}$ZSM-5 species increased gradually in intensity until 773 K (Figure 1c−h) patterning the IR results. This indicates that temperature strongly favors formation of the bound nitrosonium $NO^{\delta+}$ intermediates and that they exhibit sufficient thermal stability to be potentially involved in the SCR process. The IR experiments showed also that the band at 1900 cm^{-1} assigned to the mononitrosyl complexes, in contrast to the dinitrosyls, is the most resistant to evacuation and persists until 773 K (Figure 2d). Upon evacuation at 773 K, the $\{Ni-NO\}^{2+}$ZSM-5 adducts are largely destroyed, and QMS analysis of the gas products revealed formation of N_2O and N_2 but not the O_2 molecules. Evidently, part of the oxygen species coming from the NO disintegration remains on the catalyst surface. Within the tenets of the mechanism elaborated for the silica-grafted nickel catalyst,[18] such observations imply that the N−N bond formation step of the NO decomposition into the constituting elements was successfully accomplished. However, the O−O bond-making process, leading to dioxygen formation for eventual closing of the catalytic cycle, was apparently not yet concluded in such conditions. Therefore, to remove the residual oxygen from the catalyst surface, the presence of reductor molecules is needed.

3.2. Interaction of Ni^+ZSM-5 with CO, C_3H_6, and O_2 . After reaction with CO above 450 K, reduction of the Ni^{2+} centers to Ni^+ was observed manifested by the formation of a complex EPR spectrum (Figure 4a) because of the various types of paramagnetic polycarbonyl adducts $\{Ni^+-(CO)_n\}$ZSM-5 ($n = 1 \div 4$) of nickel(I) depending on the residual CO pressure. Their attribution was based on the response of the corresponding EPR signals to pressure and temperature variations, computer simulation of the EPR spectra supported by DFT calculations, and reference literature data for a similar Ni/SiO_2 system.[49,50] The following spin-Hamiltonian parameters for each component signal were determined: $g_{xx}^1 = 2.432$, $g_{yy}^1 = 2.376$, $g_{zz}^1 = 2.022$ and $g_{xx}^2 = 2.451$, $g_{yy}^2 = 2.376$, $g_{zz}^2 = 2.014$ (for two distinct monocarbonyl species); $g_{xx} = 2.070$, $g_{yy} = 2.076$, $g_{zz} = 2.227$ (for dicarbonyl adducts); $g_{xx} = 2.204$, $g_{yy} = 2.161$, $g_{zz} = 2.012$ (for tricarbonyl adducts); and $g_{xx} = g_{yy} = 2.127$, $g_{zz} = 2.011$ (for tetracarbonyl adducts). The electronic nature of the g tensors characteristic of the individual nickel(I) carbonyl complexes was discussed thoroughly by us in a previous paper.[50] Since all the carbonyl complexes remained in a dynamic equilibrium, the recorded EPR spectra were constituted by the superposition of several signals because of coexisting nickel(I) carbonyl species. In the corresponding IR spectra, a set of bands located in the range of 2150−2075 cm^{-1} is visible (Figure 2b) with the doublet at 2137 and 2092 cm^{-1} being the highest in intensity. The later one is characteristic of the geminal dicarbonyl $\{Ni^+-(CO)_2\}$ZSM-5 species.[45] For the lowest CO pressures, a shoulder at 2102 cm^{-1} was attributed to the monocarbonyl species $\{Ni^+-CO\}$ZSM-5 in agreement with earlier data.[45] At higher CO pressures, the gas-phase signal obscures the observation of the higher polycarbonyls by IR, although clear bands located at 2156, 2124, and 2112 cm^{-1}, growing in intensity at the expense of the dicarbonyl doublet, can be distinguished and attributed to the tricarbonyl $\{Ni^+-(CO)_3\}$ZSM-5 species.[45]

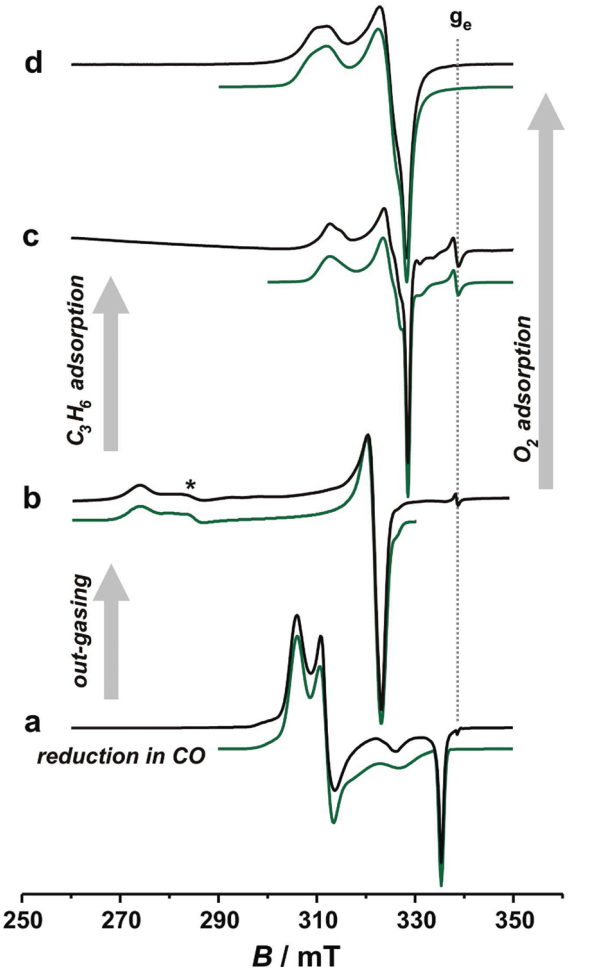

Figure 4. X-band experimental (black line) and simulated (green line) EPR spectra of the NiZSM-5 sample recorded at 77 K after (a) reduction in 20 Torr CO at 673 K for 15 min, (b) subsequent evacuation of CO (asterisk indicates the g feature of a residual monocarbonyl species), (c) 10 Torr of propene adsorbed on the reduced sample, and (d) 2 Torr of O_2 adsorbed on the reduced sample.

As an example, the optimized structure of the most abundant dicarbonyl $\{Ni^+-(CO)_2\}$M7 complex is shown in Figure 3b. The calculated adsorption energy is $\Delta E_{ads} = -63.1$ kcal/mol (with respect to separated Ni^+M7 and $2CO_{(g)}$) indicating formation of a strongly bound stable 17-electron complex. This complex exhibits tetrahedral arrangement of the Ni(I) center with two linear CO ligands at the average distance of 1.80 Å. The C−O bond lengths of 1.15 Å in the carbonyl moieties are slightly shortened with respect to the gas-phase CO (1.155 Å). The

Table 1. Summary of Spectroscopic Parameters of the Individual Intrazeolitic Complexes Observed During SCR of NO with Propene over NiZSM-5 Zeolite

structure	g_{xx}	g_{yy}	g_{zz}	ν/cm^{-1}		
Ni^{+}ZSM-5	2.110	2.110	2.482			
	2.103	2.103	2.478			
$\{Ni-NO\}^{2+}$ZSM-5	2.157	2.200	2.355	1902		
	2.145	2. 233	2.370	1896		
$\{Ni^{2+}-CO\}$ZSM-5				2212		
				2207		
$\{Ni^{+}-CO\}$ZSM-5	2.432	2.376	2.022	2102		
	2.451	2.376	2.014			
$\{Ni^{+}-(CO)_2\}$ZSM-5	2.070	2.076	2.227	2137	2092	
$\{Ni^{+}-(CO)_3\}$ZSM-5	2.204	2.161	2.012	2156	2124	2112
$\{Ni^{+}-C_3H_6\}$ZSM-5	2.067	2.090	2.177			
	2.049	2.079	2.153			
$\{Ni^{2+}-O_2^{-}\}$ZSM-5	2.065	2.085	2.170			
	2.078	2.091	2.195			

calculated frequencies of the bonded CO molecules (2124 and 2069 cm^{-1}) fit very well to the corresponding experimental values (Table 1). The spin-density contour of the $\{Ni^{+}-(CO)_2\}$M7 adduct resembles the shape of a $d_{x^2-y^2}$ state (Figure 3b), while the calculated (B3LYP-SOMF) *g*-tensor components of $g_{xx} = 2.070$, $g_{yy} = 2.094$, and $g_{zz} = 2.206$ are close to the experimental values confirming the correct structure assignment.

After prolonged evacuation of the reduced samples, the carbonyl complexes were destroyed and a well pronounced axial signal due to the isolated Ni(I) centers[51] with $g_{xx}^{1} = g_{yy}^{1} = 2.110$, $g_{zz}^{1} = 2.482$ and $g_{xx}^{2} = g_{yy}^{2} = 2.103$, $g_{zz}^{2} = 2.478$ was observed (Figure 4b). The $g_{xx,yy}$ feature indicated by the asterisk reveals the presence of a residual nickel(I) monocarbonyl species not destroyed by the prolonged evacuation at 550 K.

The reduced Ni^{+}ZSM-5 catalysts reacted quite easily with the adsorbed propene forming a π-complex as it was shown by the appearance of a new EPR signal (Figure 4c). Computer simulation indicated formation of two types of such complexes with $g_{xx}^{1} = 2.067$, $g_{yy}^{1} = 2.090$, $g_{zz}^{1} = 2.177$, and $g_{xx}^{2} = 2.049$, $g_{yy}^{2} = 2.079$, $g_{zz}^{2} = 2.153$. With the temperature increase, this signal changed indicating dimerization of the adsorbed propene as observed earlier[49] preserving, however, the monovalent state of nickel. As a result, simple adsorption experiments using the samples with the nickel in oxidized or reduced states disclosed high affinity of CO and propene for complexation with Ni^{+}, which is contrasted with their apparent reluctance toward adsorption on the Ni^{2+} sites.

The monovalent nickel centers provide an excellent active site for dioxygen detain. Adsorption of dioxygen on the reduced Ni^{+}ZSM-5 samples led to a development of an orthorhombic EPR signal (Figure 4d) with $g_{xx}^{1} = 2.065$, $g_{yy}^{1} = 2.085$, $g_{zz}^{1} = 2.170$ and $g_{xx}^{2} = 2.078$, $g_{yy}^{2} = 2.091$, $g_{zz}^{2} = 2.195$ characteristic of bound O_2^{-} superoxide radicals. They are produced along a metal-to-ligand electron transfer (MLET) route following the equation

$$^{3}O_2 + {}^{2}Ni^{+}\text{ZSM-5} \rightarrow {}^{2}\{Ni^{2+}-O_2^{-}\}\text{ZSM-5} \qquad (2)$$

DFT calculations of the nickel(I)-bound superoxide radicals indicated that the most stable ($\Delta E_{ads} = -46.9$ kcal/mol) conformation of the $\{Ni^{2+}-O_2^{-}\}$M7 cluster exhibits an η^2 binding mode of the ligand (Figure 3c). The resulting planar 4-fold coordination of the metal center is featured by the side-on ligation of the superoxide species forming two nearly equivalent bonds with the nickel core (1.804 and 1.796 Å). Two other nickel−zeolite bonds are equal to 1.947 and 1.913 Å. The optimized geometry of the adduct gives rise to peculiar spin density distribution between the superoxide moiety and the nickel core with a pronounced part confined to the metal center ($\rho_{Ni} = 0.36$, $\rho_O = 0.32$, $\rho_O = 0.30$). Changes in the atomic charge distribution within the $\{Ni^{2+}-O_2^{-}\}$ unit with respect to the separated O_2 and Ni^{+}M7 ($\Delta q_{Ni} = 0.32$, $\Delta q_O = -0.10$, $\Delta q_O = -0.11$) confirm the MLET mechanism of dioxygen activation. As a result, the calculated *g*-tensor components are larger than in the case of the electrostatically bound O_2^{-} species.[52] The calculated values obtained within the BP-SOMF scheme ($g_{xx} = 2.039$, $g_{yy} = 2.098$, $g_{zz} = 2.178$), being in good agreement with the experiment, prove the η^2 nature of the observed superoxide species.

In the presence of gas-phase NO, the superoxide radicals are immediately converted into diamagnetic surface NO_3^{-} species ($O_2^{-}{}_{zeol} + NO_{(g)} \rightarrow NO_3^{-}{}_{zeol}$) revealed by IR on the basis of the positions of the diagnostic bands at $\nu = 1600$ and 1491 cm^{-1}.[30] The latter intermediates have been widely examined in the context of hydrocarbon assisted SCR as oxidant species.[4,9,13,26,30] The spectroscopic EPR and IR parameters obtained after interaction of NO, C_3H_6, CO, and O_2 with the Ni^{2+} and Ni^{+} centers are summarized and are listed in Table 1.

A précis of the obtained results indicates that in the SCR process the reduced nickel(I) sites may act as the bifunctional centers, which easily coordinate and activate both the hydrocarbon (as well as CO) reductor and the O_2 oxidant species in a competitive way. Therefore, reductive adsorption of NO on the nickel(II) sites can facilitate subsequent coordination of hydrocarbons for their further inner-sphere conversion implicated in the nitric oxide reduction process (vide infra).

3.3. Variable Temperature EPR Study of the SCR Process. To verify the relevance of the described model reactions with single reactants for the real HC-SCR process, the reaction of NiZSM-5 catalyst with a mixture of C_3H_6 (5 Torr), O_2 (2 Torr), and NO (6 Torr) in the temperature range of 295−773 K was monitored with EPR and QMS spectroscopies (for the sake of better resolution, the spectra were recorded after quenching at 77 K). The investigations were performed for the *R* coefficient ≤0.2 corresponding to the reducing conditions. The value of this coefficient was calculated from the formula proposed by Tanaka et al.[53] as $R = ([NO] + 2[O_2])/9[C_3H_6]$.

To promote the SCR reaction, the parent oxidized Ni^{2+}ZSM-5 sample was progressively heated up to 773 K in the presence of the reactant mixture, and the EPR spectra were recorded sequentially. Upon admission of propene at room temperature, no relevant EPR signals were detected (Figure 5a). However, after subsequent addition of NO and O_2 to the reaction mixture and heating the sample in the temperature rage 295−473 K, gradual development of the EPR signal due to the $\{Ni-NO\}^{2+}$ZSM-5 complexes was observed (Figure 5b). It indicated that among all SCR reactants present in the gas mixture only the nitric oxide was selectively captured by Ni^{2+} sites and was activated into the nitrosonium $NO^{\delta+}$ species. Upon increase of the temperature to 673 K, this signal still persisted (Figure 5c). Further heating of the sample at 773 K for 15 min led to the dramatic changes in the EPR spectrum. The signal of the $\{Ni-NO\}^{2+}$ZSM-5 completely disappeared, and a complex spectrum due to the polycarbonyl adducts of nickel(I), easily

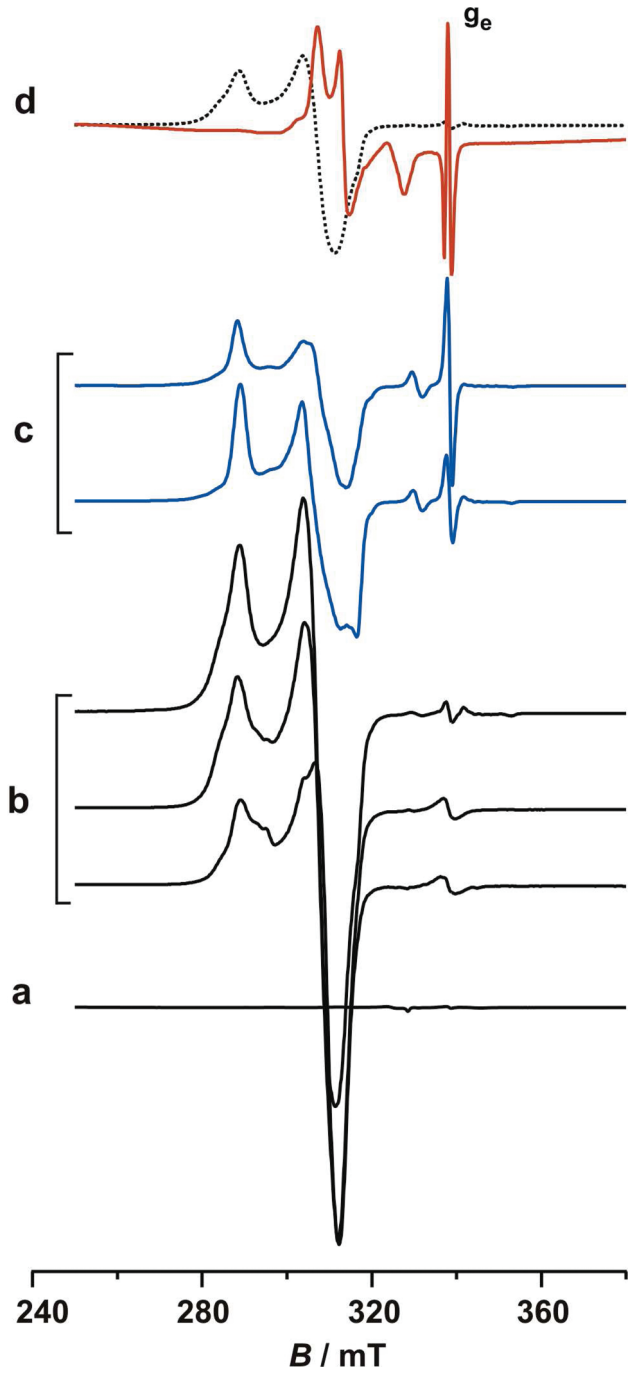

Figure 5. In-situ EPR spectra (77 K) recorded during SCR of NO with propene over NiZSM-5 catalyst. (a) Adsorption of 5 Torr of propene, (b) thermal evolution between 300 and 483 K after coadsorption of 5 Torr of propene, 2 Torr of O_2, and 6 Torr of NO, (c) change of the signal between 573 and 673 K, and (d) after reaction at 773 K (the dotted spectrum shows the $\{Ni{-}NO\}^{2+}$ZSM-5 signal at the reaction temperature without O_2 and propene).

recognized thanks to the spectroscopic signatures known from the previous model studies, was observed (Figure 5d). The dotted line in Figure 5d shows the intensity of the $\{Ni{-}NO\}^{2+}$ZSM-5 signal recorded after treatment at 773 K in the absence of other reactants proving to be a useful reference for its thermal stability in such conditions. The same sequence of the EPR spectra was observed when NO_2 was used instead of NO in accordance with the dissociative character of nitrogen dioxide adsorption described above.

The above results indicate that propene presumably π-bonded to reduced nickel core of the $\{Ni{-}NO\}^{2+}$ species, even in the presence of oxygen, can be oxidized by the nitrosonium species to CO_x, and the resultant carbon monoxide molecules are trapped by the reduced nickel(I) centers in the form of the carbonyl complexes. Admission of excess oxygen led to the disappearance of all signals and reoxidation of the catalytic centers to Ni^{2+}. Subsequent QMS analysis of the gas products showed the presence of N_2, H_2O, and CO_2/CO and the absence of any other nitrogen-related byproduct confirming that the SCR cycle was, indeed, accomplished in such conditions. It is, thus, clear that the SCR process is initiated by the preferential adsorption of NO on the oxidized nickel centers and formation of $NO^{\delta+}$ intermediates, which are next consumed in the reaction with propene (captured subsequently by the $\{Ni{-}NO\}^{2+}$ reduced nickel core) to produce the final reaction products: N_2, CO_2/CO, and H_2O. During the whole process, the redox Ni^{2+}/Ni^{+} couple triggers the sequence of the elementary steps since the valence state of the nickel centers dictates not only the direction of the charge flow during activation of the reactants but also the ability of their selective coordination. Obviously, the proposed pathway does not disregard involvement of possible competing routes with surface nitrites and nitrates as oxidizing species proposed in the literature on the basis of sole IR data especially in the late stages of the SCR process.

4. CONCLUSIONS

By means of combined use of EPR, IR, and DFT methods, it is shown that at the SCR temperatures the interaction of NO_x with Ni^{2+} centers hosted in ZSM-5 zeolite leads to the formation of bonded nitrosonium $NO^{\delta+}$ intermediates via cooperative spin-pairing and ligand-to-metal charge-transfer process. The reduced Ni^{+} centers are prone to react easily with C_3H_6, CO, and O_2 molecules. The corresponding intermediates were identified during the selective catalytic reduction of NO with propene, which indicates that Ni^{2+}/Ni^{+} redox couple operates in the reaction course. The backbone of the SCR mechanism consists in the prompt chemoselective adsorption of NO on the nickel(II) sites initiating the catalytic cycle. The resultant nitrosyl adduct with reduced nickel core promotes subsequent coordination of hydrocarbons for their inner-sphere conversion in the presence of oxygen into the final reaction products (N_2, CO_x, H_2O).

AUTHOR INFORMATION

Corresponding Author

*Phone: +48 12 663 22 24; fax: +48 12 634 05 15; e-mail: pietrzyk@chemia.uj.edu.pl.

ACKNOWLEDGMENT

Financial support by the Ministry of Science and Higher Education (MNiSW) of Poland, Grant No. N N204 165336, is acknowledged. Dr. B. Gil (Jagiellonian University) is kindly acknowledged for recording the IR spectra. The calculations were carried out with the computer facilities of Academic Computing Center CYFRONET under Grant No. MNiSW/IBM_BC_HS21/UJ/092/2008. The research was carried out

with the equipment purchased thanks to the financial support of the European Regional Development Fund in the framework of the Polish Innovation Economy Operational Program (contract no. POIG.02.01.00-12-023/08).

REFERENCES

(1) Sulikowski, B.; Janas, J.; Haber, J.; Kubacka, A.; Olejniczak, Z.; Wloch, E. *Chem. Commun.* **1998**, *24*, 2755–2756.
(2) Wang, X.; Chen, H.-Y.; Sachtler, W. M. H. *J. Catal.* **2001**, *197*, 281–291.
(3) Santhosh Kumar, M.; Schwidder, M.; Grünert, W.; Brückner, A. *J. Catal.* **2004**, *227*, 384–397.
(4) Chen, X.; Yang, X.; Zhu, A.; Au, C. T.; Shi, C. *J. Mol. Catal. A: Chem.* **2009**, *312*, 31–39.
(5) Klingstedt, F.; Arve, K.; Eränen, K.; Murzin, D. Y. *Acc. Chem. Res.* **2006**, *39*, 273–282.
(6) Liu, Z. M.; Woo, S. I. *Catal. Rev. Sci. Eng.* **2006**, *48*, 43–89.
(7) Long, J.; Zhang, Z.; Ding, Z.; Ruan, R.; Li, Z.; Wang, X. *J. Phys. Chem. C* **2010**, *114*, 15713–15727.
(8) Xiao, F-. S.; Zheng, S.; Sun, J.; Yu, R.; Qiu, S.; Xu, R. *J. Catal.* **1998**, *176*, 474–487.
(9) Poignant, F.; Freysz, J. L.; Daturi, M.; Saussey, J. *Catal. Today* **2001**, *70*, 197–211.
(10) Mosqueda-Jiménez, B. I.; Jentys, A.; Seshan, K.; Lercher, J. A. *J. Catal.* **2003**, *218*, 375–385.
(11) Hadjiivanov, K. I. *Catal. Rev. Sci. Eng.* **2000**, *42*, 71–144.
(12) Kasai, P. H.; Bishop, R. J.; McLeod, D. *J. Phys. Chem.* **1978**, *82*, 279–285.
(13) Zhang, X.; He, H.; Gao, H.; Yu, Y. *Spectrochim. Acta, Part A* **2008**, *71*, 1446–1451.
(14) Rodriguez-Santiago, L.; Sierka, M.; Branchadell, V.; Sodupe, M.; Sauer, J. *J. Am. Chem. Soc.* **1998**, *120*, 1545–1551.
(15) Pulido, A.; Nachtigall, P. *Phys. Chem. Chem. Phys.* **2009**, *11*, 1447–1458.
(16) Pietrzyk, P.; Gil, B.; Sojka, Z. *Catal. Today* **2007**, *126*, 103–111.
(17) Ramprasad, R.; Schneider, W. F.; Hass, K. C.; Adams, J. B. *J. Phys. Chem. B* **1997**, *101*, 1940–1949.
(18) Sojka, Z.; Pietrzyk, P.; Martra, G.; Kermarec, M.; Che, M. *Catal. Today* **2006**, *114*, 154–161.
(19) Pietrzyk, P.; Sojka, Z. *Chem. Commun.* **2007**, *19*, 1930–1932.
(20) Fisicaro, P.; Giamello, E.; Berlier, G.; Lamberti, C. *Res. Chem. Intermed.* **2003**, *29*, 805–816.
(21) Solymosi, F.; Bánsági, T. *J. Catal.* **1995**, *156*, 75–84.
(22) Meunier, F. C.; Zuzaniuk, V.; Breen, J. P.; Olsson, M.; Ross, J. R. H. *Catal. Today* **2000**, *59*, 287–304.
(23) Giamello, E.; Murphy, D.; Magnacca, G.; Morterra, C.; Shioya, Y.; Nomura, T.; Anpo, M. *J. Catal.* **1992**, *136*, 510–520.
(24) Groothaert, M. H.; Bokhoven, J. A.; Battison, A. A.; Weckhuysen, B. M.; Schoonheydt, R. A. *J. Am. Chem. Soc.* **2003**, *125*, 7629–7640.
(25) Pérez-Ramírez, J.; Kapteijn, F.; Mul, G.; Mulijn, J. A. *Appl. Catal., B: Environ.* **2002**, *35*, 227–234.
(26) Sadovskaya, E. M.; Suknev, A. P.; Pinaeva, L. G.; Goncharov, V. B.; Bal'zhinimaev, B. S.; Chupin, C.; Pérez-Ramírez, J.; Mirodatos, C. *J. Catal.* **2004**, *225*, 179–189.
(27) De Lucas, A.; Valverde, J. L.; Dorado, F.; Romero, A.; Asencio, I. *J. Mol. Catal. A: Chem.* **2005**, *225*, 47–58.
(28) Li, Y.; Armor, J. N. *Appl. Catal., B: Environ.* **1993**, *2*, 239–256.
(29) Tang, J.; Zhang, T.; Ma, L.; Li, L.; Zhao, J.; Zheng, M.; Lin, L. *Catal. Lett.* **2001**, *73*, 193–197.
(30) Mihaylov, M.; Hadjiivanov, K.; Panayatov, D. *Appl. Catal., B: Environ.* **2004**, *51*, 33–42.
(31) Wichterlová, B.; Sobalik, Z.; Dďdeček, J. *Appl. Catal., B: Environ.* **2003**, *41*, 97–114.
(32) Pietrzyk, P.; Zasada, F.; Piskorz, W.; Kotarba, A.; Sojka, Z. *Catal. Today* **2007**, *119*, 219–227.
(33) Hadjiivanov, K.; Tsyntsarski, B.; Venkov, T.; Daturi, M.; Saussey, J.; Lavalley, J.-C. *Phys. Chem. Chem. Phys.* **2003**, *5*, 1695–1702.
(34) Louis, C.; Sojka, Z.; Che, M. *J. Chem. Soc., Faraday Trans. 1* **1989**, *85*, 3939–3952.
(35) Pöppl, A.; Rudolf, T.; Manikandan, P.; Goldfarb, D. *J. Am. Chem. Soc.* **2000**, *122*, 10194–10200.
(36) Brückner, A. *Catal. Rev. Sci. Eng.* **2003**, *45*, 97–150.
(37) Spalek, T.; Pietrzyk, P.; Sojka, Z. *J. Chem. Inf. Model.* **2005**, *45*, 18–29.
(38) *ADF2005.01, SCM, Theoretical Chemistry*; Vrije Universiteit: Amsterdam, The Netherlands, 2005 (http://www.scm.com).
(39) (a) Becke, A. D. *Phys. Rev. A* **1988**, *38*, 3098–3100. (b) Perdew, J. P. *Phys. Rev. B* **1986**, *33*, 8822–8824.
(40) Neese, F. *ORCA—An Ab Initio, DFT and Semiempirical Electronic Structure Package*, version 2.6-04.2007; Universität Bonn: Bonn, Germany, 2007.
(41) Neese, F. *J. Chem. Phys.* **2001**, *115*, 11080–11097.
(42) Stephens, P. J.; Devlin, F. J.; Chabalowski, C. F.; Frisch, M. J. *J. Phys. Chem.* **1994**, *98*, 11623–11627.
(43) Neese, F. *J. Chem. Phys.* **2007**, *127*, 164112–164120.
(44) Krzystek, J.; Park, J-. H.; Meisel, M. W.; Hitchman, M. A.; Stratemeier, H.; Brunel, L-. C.; Telser, J. *Inorg. Chem.* **2002**, *41*, 4478–4487.
(45) Hadjiivanov, K.; Knozinger, H.; Mihaylov, M. *J. Phys. Chem. B* **2002**, *106*, 2618–2624.
(46) Gutsze, A.; Plato, M.; Karge, H. G.; Witzel, F. *J. Chem. Soc., Faraday Trans.* **1996**, *92*, 2495–2498.
(47) Chiesa, M.; Paganini, M. C.; Giamello, E.; Di Valentin, C.; Pacchioni, G. *J. Mol. Catal. A: Chem.* **2003**, *204—205*, 779–786.
(48) Adamski, A.; Tabor, E.; Gil, B.; Sojka, Z. *Catal. Today* **2007**, *119*, 114–119.
(49) Bonneviot, L.; Olivier, D.; Che, M. *J. Mol. Catal.* **1983**, *21*, 415–430.
(50) Pietrzyk, P.; Podolska, K.; Sojka, Z. *J. Phys. Chem. A* **2008**, *112*, 12208–12219.
(51) Serykh, A. I.; Amiridis, M. D. *J. Phys. Chem. C* **2007**, *111*, 17020–17024.
(52) Chiesa, M.; Giamello, E.; Paganini, M. C.; Sojka, Z.; Murphy, D. M. *J. Chem. Phys.* **2002**, *116*, 4266–4274.
(53) Tanaka, T.; Kokota, K.; Isomura, N.; Doi, H.; Sugiura, M. *Appl. Catal., B: Environ.* **1998**, *16*, 199–208.